# Measurement of absolute radical densities in a plasma using modulated-beam line-of-sight threshold ionization mass spectrometry

Sumit Agarwal
*Department of Chemical Engineering, University of California, Santa Barbara, California 93106-5080*

Guido W. W. Quax and M. C. M. van de Sanden
*Department of Applied Physics, Eindhoven University of Technology, P.O. Box 513, 5600 MB, Eindhoven, The Netherlands*

Dimitrios Maroudas
*Department of Chemical Engineering, University of Massachusetts, Amherst, Massachusetts 01003-3110*

Eray S. Aydil[a)]
*Department of Chemical Engineering, University of California, Santa Barbara, California 93106-5080*

(Received 7 August 2003; accepted 29 September 2003; published 25 November 2003)

Using modulated beam line-of-sight threshold ionization mass spectrometry (LOS-TIMS) we measured absolute O, $O_2$, and Ar densities, and the average neutral-gas temperature in an $O_2/Ar$ electrical discharge as a function of pressure in the plasma chamber and the mole fraction of Ar in $O_2$; the pressure and mole fraction range was 25–200 mTorr and 0–0.90, respectively. Although LOS-TIMS is a versatile tool for measuring absolute radical densities, it requires careful vacuum design and calibration to account for various sources of error such as the contribution to the quadrupole mass spectrometer (QMS) ion current from the background gases, the ion mass-to-charge ratio dependent sensitivity of the various QMS components, and space-charge limitations in the QMS ionizer. In addition, collisions within the molecular beam extracted from the discharge must be taken into account particularly for higher plasma chamber pressures ($>75$ mTorr). In our measurements, these effects are carefully considered and the consequences of ignoring them are discussed. The O atom density increases with pressure and $O_2$ mole fraction in the feed gas and is in the range of $2.1\times10^{18}$–$2.6\times10^{19}$ $m^{-3}$. At low pressures, our measurements show that the $O_2$ translational temperature is higher than that for Ar. © *2004 American Vacuum Society.* [DOI: 10.1116/1.1627767]

## I. INTRODUCTION

Measurement of radical densities in an electrical gas discharge is important for understanding and improving plasma etching and plasma-assisted deposition processes. Absolute density measurements are also needed for testing the reliability of reactive plasma models. Various plasma diagnostic methods based on ultraviolet, visible, vibrational, and ionization spectroscopies, and chemical titration methods have been used for radical density measurements in plasmas.[1,2] Among the various techniques used for measuring radical densities, threshold ionization mass spectrometry (TIMS)[2–11] is particularly useful since it enables the determination of the densities of all the radicals in the discharge near the substrate surface. In contrast, optical techniques are limited by the availability of accessible excited states of the radical and sometimes provide spatially averaged densities over the plasma volume. Although TIMS is a versatile tool for measuring absolute radical densities, it requires careful vacuum design and calibration which should take into account various sources of error: these include the ion mass-to-charge ratio dependence in the sensitivity of the various components in the quadrupole mass spectrometer (QMS),[8,9] space-charge limitations in the QMS ionizer,[12–15] as well as the collisions in the molecular beam extracted from the discharge. The latter correction is particularly important for higher operating pressures in the plasma chamber, where the mean free path in the beam is smaller than the extraction orifice dimensions ($>75$ mTorr in this study).

In line-of-sight TIMS (LOS-TIMS), the species in the plasma are sampled through a small aperture on the chamber wall or the substrate stage as shown in Fig. 1. The mass spectrometer is placed in line-of-sight with this aperture in a differentially pumped chamber where the mean free path is greater than the characteristic length of the QMS housing. This ensures that after extraction the plasma species reach the mass spectrometer ionizer without any collisions with the walls of the chamber that houses the QMS. The QMS accepts only a small solid angle of the species sampled from the aperture on the plasma chamber, which constitutes the *beam component* of the species that enter the ionizer. Any species sampled from the plasma that are not within the solid angle of this beam, reach the QMS after several collisions with the walls of the housing resulting in the *background component* of the signal. Thus, the QMS ion current (henceforth referred to as the QMS signal) resulting from the beam component is always superimposed onto a QMS signal resulting from the background gas due to the finite pressure in

[a)]Author to whom correspondence should be addressed; electronic mail: aydil@engineering.ucsb.edu

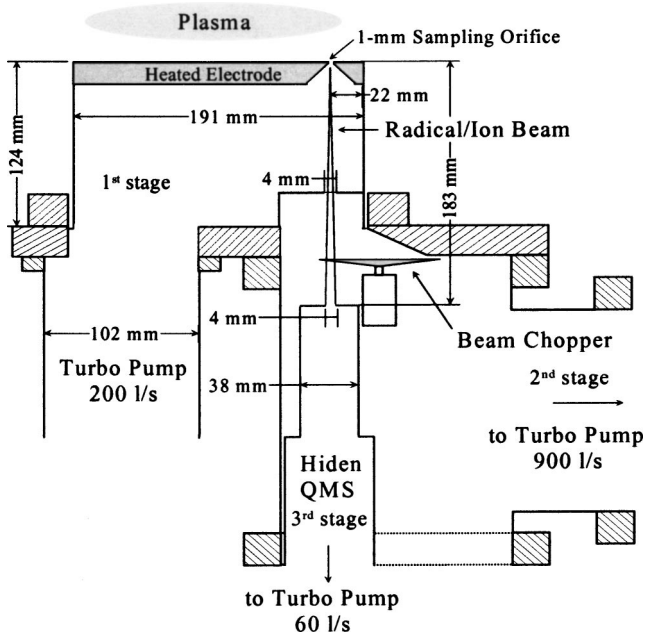


FIG. 1. Schematic of the three-stage differentially pumped line-of-sight housing for the quadrupole mass spectrometer equipped with a Bessel-box-type ion-energy analyzer.

the differentially pumped chamber that houses the QMS. In most applications for TIMS, several stages of differential pumping are required to obtain a high beam-to-background ratio.[8] Furthermore, beam modulation is also required to separate the beam component of the signal from the background signal.[8]

In this article, we present our design of the three-stage differentially pumped housing for the quadrupole mass spectrometer (QMS) for conducting modulated-beam line-of-sight TIMS measurements. We also present a calibration procedure for obtaining absolute radical densities, parent molecule densities, and the neutral-gas temperature at the sampling aperture, from the QMS signal, based on a method similar to that suggested by Singh, Coburn, and Graves.[9,16] We have used an $O_2$/Ar plasma as the prototypical system and present specific results obtained as a function of plasma chamber pressure and $O_2$-to-Ar ratio in the feed gas.

The organization of this article is as follows. In Sec. II, we describe our experimental setup placing emphasis on the various design considerations for the QMS housing. In Sec. III, we describe the principle of TIMS and the details of the calibration procedure and various corrections required for obtaining reliable absolute radical density measurements. In Sec. IV, we present specific results for the $O_2$/Ar plasma, and finally, in Sec. V, we summarize the conclusions of our study.

## II. EXPERIMENT

### A. Plasma reactor and the QMS housing

The plasma reactor used in this study has been discussed in detail previously.[17] Briefly, the experiments were conducted in a stainless steel, inductively coupled plasma (ICP) reactor. The plasma was generated by applying radio-frequency (rf) power at 13.56 MHz to a planar spiral coil seated on a quartz window, which forms the vacuum seal. The rf power to the plasma source was kept at 500 W. The plasma chamber was pumped by a 900 $l/s$ turbomolecular pump (Leybold TMP 1000) which provided a base pressure of $\sim 10^{-7}$ Torr. The feed gases were injected through a gas injection ring close to the plasma source and the gas flow rates were controlled by mass flow controllers (BOC Edwards Model 825 Series B). The total gas flow rate was kept constant at 50 standard $cm^3$/min (sccm) while the concentration of Ar in terms of mole percentage was varied from 0% to 90% Ar in $O_2$. The pressure in the chamber was measured by a capacitance manometer (BOC Edwards Model 655) and regulated by a throttle valve and a downstream adaptive pressure controller (VAT PM-5). In this study, the pressure range in the plasma chamber was varied from 25 to 200 mTorr for all the $O_2$/Ar feed–gas ratios.

A schematic of the three-stage differentially pumped housing for the QMS is shown in Fig. 1. The gas-phase species in the plasma were sampled through a 1 mm aperture on the substrate platen. The distance between the quartz window and the grounded substrate was approximately 20 cm. The sampling aperture was placed off-axis on the substrate to provide sufficient space for the 200 $l/s$ turbomolecular pump (Osaka TG 203) for the first stage of differential pumping as shown in Fig. 1. The effective pumping speed for this stage was estimated to be 150 $l/s$. A cold-cathode gauge (Varian NRC 524-2) was used to monitor the pressure in the first stage and the pressure was in the range $10^{-6}$–$10^{-5}$ Torr for 25–200 mTorr operating pressure in the plasma chamber. A 4-mm-diameter aperture separated the first and second stages of differential pumping. A 900 $l/s$ turbomolecular pump (Leybold TMP 1000) was used to differentially pump the second stage. The QMS (Hiden PSM-2) coupled with an in-line "Bessel Box" type ion-energy analyzer[18,19] was placed directly in the beam path and the inside of the QMS provided third differentially pumped stage (Fig. 1). The QMS probehead had a 4 mm orifice separating the second and third stages of differential pumping. The QMS was pumped by a 56 $l/s$ turbomolecular pump (Balzers TPU 60). The pumping speed in the third stage was conductance limited and was estimated to be 10 $l/s$. The pressure in the QMS was measured by a Bayard–Alpert-type ionization gauge and was almost independent of the pressure in the plasma chamber for the range of pressures used in this study. The pressure in the QMS during plasma operation was $\sim 10^{-8}$ Torr and the base pressure after baking was $\sim 10^{-9}$ Torr. The total distance between the orifice on the plasma chamber and the orifice on the QMS was 18.3 cm resulting in a solid angle of 1.25° for the beam. All the orifices were drilled after assembling the entire QMS housing to ensure that the center of each orifice was perfectly aligned along the same vertical axis. A chopper was used to modulate the beam to separate the beam and background components. The chopper was a dc electric motor compatible with high vacuum (Globe Motors 41A100:M41M45) with two 90° arc blades that were used to

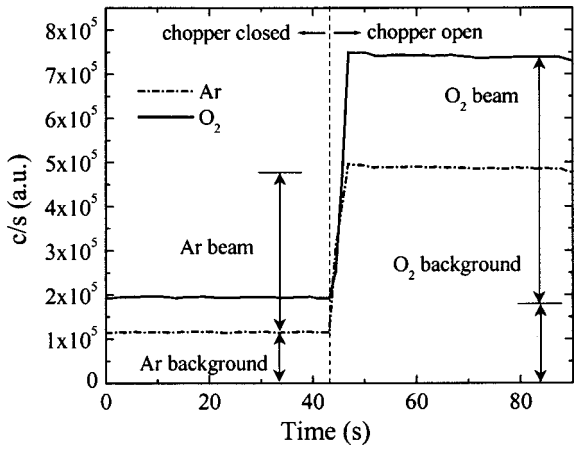


FIG. 2. QMS signals for $O_2^+$ (—) and $Ar^+$ (- - -) at an electron energy of 35 eV and electron emission current of 120 $\mu$A collected with the chopper in the open (beam+background) and closed (background) positions for a feed–gas composition of 70% $O_2$ and 30% Ar and a pressure of 100 mTorr in the plasma chamber. Plasma was off. The signal levels corresponding to Ar and $O_2$ from the plasma chamber (beam), and Ar and $O_2$ from the background are shown.

block the beam. The position of the chopper was determined by the change in the QMS signal for the parent species as the chopper was rotated and stopped at either the chopper-open or chopper-closed positions; this is illustrated in Fig. 2 and will be discussed further in Sec. II B.

### B. Design considerations

The beam component forms only a small fraction of the exit cosine distribution (for ideal molecular flow)[20] of the species sampled from the aperture on the wall of the plasma chamber. Species outside this solid angle contribute to the background component. Design of the QMS housing requires a balance between maximizing the beam signal and suppressing the background component by employing multiple stages of differential pumping. Using several stages of differential pumping, most of the species in the background can be pumped out before they reach the ionizer of the QMS. This results in a low but finite pressure in the ionizer, which in turn results in a spurious background signal of radicals. There are primarily two sources for the background radical signal. First, the neutral species in the QMS ionizer are pyrolyzed on the hot filament ($\sim$1800 K) resulting in radicals that can be subsequently ionized and detected. Second, radical species that have a low sticking probability on stainless steel can survive several bounces on the walls of the mass spectrometer housing, reach the QMS ionizer, and get detected. These sources of background can result in a substantial overestimation of the beam component.[8] A chopper is used to modulate the beam to separate the beam signal from the background; this will be discussed in more detail in Sec. III A. Although the background signal is suppressed by using several stages of differential pumping, this results in a longer beam path due to geometric constraints of accommodating pumps and, thus, reduces the solid angle of the beam sampled by the QMS. Therefore, the number of stages of differential pumping and the length of the beam path should be chosen such that the beam signal is above the sensitivity limit of the QMS and there is a sufficient beam-to-background pressure ratio to differentiate the beam signal from the superimposed background. The diameter of the extraction orifice on the wall of the plasma chamber can be used to increase the beam signal, but it should not be so large that the plasma is perturbed by the presence of the orifice.

Our QMS housing has a line-of-sight geometry in which the sampling orifice on the substrate platen of the plasma chamber, the ionizer of the QMS, and the secondary electron multiplier (SEM) lie along the same axis. This ensures that all the species that are sampled from the extraction orifice of the plasma chamber reach the detector without any collisions with the wall of the housing. In order to avoid any spurious signal resulting from photons and other radiation emanating from the plasma, the QMS is equipped with an in-line Bessel-box-type ion-energy analyzer[18,19,21–23] which bends the ions (created in the ionizer) around an obstruction via an electrostatic field but stops any radiation from reaching the SEM.

We have used modulated-beam mass spectrometry to separate the beam and background components of the QMS signal using a chopper. However, it is critical that beam modulation should not result in the modulation of the background component itself. When the chopper blocks the beam, it can result in a modulation of pressure in the ionizer of the QMS as the particles in the beam now contribute to the background. Therefore, the chopper was placed in the second differential pumping stage, where the beam pressure is low enough ($\sim 10^{-7}$ Torr) to minimize this effect.

The beam-to-background ratio for our setup for nonreactive species is demonstrated in Fig. 2, where the QMS signal for $O_2^+$ ($m/e=32$) and $Ar^+$ ($m/e=40$) in counts/s is plotted as a function of time with the chopper in the open and closed positions while the discharge was left off. The beam-to-background ratio depends on the pressure in the plasma chamber, the molecular weight of the gas, and the feed–gas ratio. For pure $O_2$ in the plasma chamber, the beam-to-background ratio for $O_2$ varied from 3.2 at 25 mTorr to 2.0 at 200 mTorr pressure. However, for 90% Ar and 10% $O_2$ in the feed gas, the beam-to-background ratio for $O_2$ was 2.4 at 25 mTorr and 2.3 at 200 mTorr. For nonreactive species, the source of background signal is the residual gas pressure in the QMS ionizer. This residual pressure for gas mixtures depends on the relative pumping speed of the different gases. Hence, a different beam-to-background ratio is obtained for each gas for different feed–gas ratios. The beam-to-background ratio for O radicals depends on the amount of O generated in the plasma chamber. For O radicals, the primary source of the background signal was O generated on the filament of the ionizer due to thermal pyrolysis of $O_2$ to form O radicals. The signal due to O radicals in the background gas was very small due to the high recombination probability of O radicals on stainless steel.[24] For pure $O_2$ in the plasma chamber, the beam-to-background ratio for O varied from 5.5 at 25 mTorr to 5.7 at 200 mTorr. For 90% Ar and 10% $O_2$

in the feed gas, the number density of O in the plasma was lower resulting in a smaller beam-to-background ratio; it was 1.8 at 25 mTorr and 3.4 at 200 mTorr.

## III. TIMS PRINCIPLE AND CALIBRATION OF THE QMS SIGNAL TO OBTAIN ABSOLUTE RADICAL DENSITIES

### A. Principle of TIMS

In mass spectrometry, electron impact ionization of a radical and its parent molecule can result in the same ion. For example, $O^+$ ions can be formed by both, direct ionization of O radicals:

$$O+e\rightarrow O^+ +2e, \quad (E_1=13.8\ \text{eV}), \tag{1}$$

and through dissociative ionization of $O_2$ molecules:

$$O_2+e\rightarrow O^+ +O+2e, \quad (E_2=18.0\ \text{eV}). \tag{2}$$

The energies in parentheses, $E_1$ (Ref. 25) and $E_2$,[26] are the threshold energies for the ionization processes in Eqs. (1) and (2), respectively. The direct ionization process always has a lower threshold than the dissociative ionization process and the difference in the thresholds for the two processes is typically equal to the binding energy of the bond that is broken during dissociative ionization. In TIMS, radicals sampled from the plasma are ionized by energetic electrons with varying energy and the resulting ionic species are subsequently detected by a QMS. The difference in the thresholds for direct and dissociative ionization enables the distinction of the QMS signal due to the radical species, O, from its parent molecule, $O_2$, in the electron impact energy range of 13.8–18.0 eV. This principle for radical detection, i.e., using a mass spectrometer with a variable electron energy source to differentiate ions created by direct ionization from those that are formed by dissociative ionization, is the fundamental principle upon which TIMS is based.

For example, Fig. 3 shows the QMS signal for $O^+$ ions ($m/e=16$) as a function of electron energy for the chopper-open and chopper-closed positions with the plasma maintained at 100 mTorr and a feed–gas composition of 90% $O_2$ and 10% Ar. The electron energy scans were made in increments of 0.1 eV. In Fig. 3, the threshold for direct ionization is indicated by the lowest energy at which ions are detected and the threshold for dissociative ionization is indicated by the change in slope of the curve; this change in slope can be clearly observed in Fig. 3 with the chopper in both open and closed positions. Ideally, there should be no $O^+$ signal detected by the QMS between the thresholds for direct and dissociative ionization in the chopper-closed position (background) since O radicals are expected to be produced only in the plasma. However, there is a background contribution to the signal from O radicals (see also Sec. II B) due to the thermal dissociation of $O_2$ on the hot filament in the ionizer and O radicals in the background gas that enter the ionizer after collisions with the walls. In order to differentiate the radical signal due only to the beam component, we take the difference between the QMS signals measured with the chopper in the open and closed positions. After subtraction, a few electron volts above the threshold for direct ionization, the QMS signal for $O^+$ is several hundred counts/s, i.e., well above the sensitivity of the QMS ($\sim$20 counts/s). It should be noted that the electron–energy scale on the Hiden QMS also requires calibration. We have used the well-known thresholds for parent ionization of Ar at 15.6 eV and $N_2$ at 15.58 eV to adjust the electron energy scale. For all gases used in our study, we found that the energy scale was offset by $+1.8$ eV for the appearance potential.

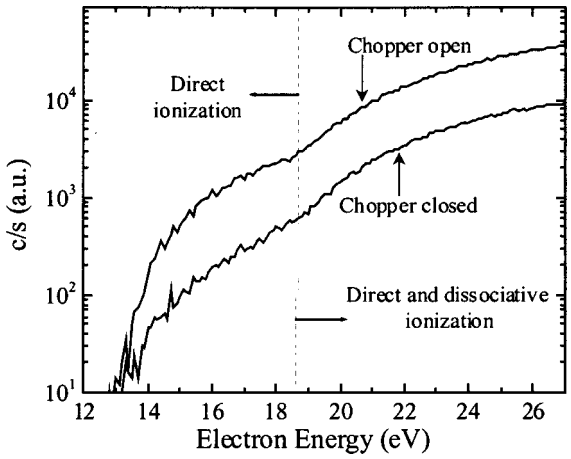


FIG. 3. QMS signal for $O^+$ ($m/e=16$) measured with the plasma maintained at 100 mTorr as a function of electron energy (plotted on a semi-log scale) for the chopper-open and chopper-closed positions. The feed–gas composition was 90% $O_2$ and 10% Ar. The data clearly show the threshold for direct ionization of O to $O^+$ at 13.6 eV. The threshold for the dissociative ionization of $O_2$ to $O^+$ is apparent from the break in the slope at $\sim$19 eV.

### B. Space-charge limitations in the ionizer

During TIMS, the QMS signal has to be recorded by varying only the electron energy in the ionizer while maintaining a constant filament electron emission current, which is a measure of the flux of electrons incident onto the radical beam in the ionizer. However, if the emission current is set too high, the electrons emitted from the filament and the electrons generated by the ionization process are not accelerated fast enough to the positively biased ionization cage resulting in a space-charge region in the ionizer. In such a case, the maximum emission current, $I_{CL}$, that can be extracted from the filament becomes a function of the electron energy, $E$, and is given by the Child–Langmuir law,[27] $I_{CL}=B_O\cdot E^{3/2}$, where $B_O$ is a constant determined by the geometry of the ionizer. If the QMS ionizer is operated in the space-charge limited regime, it will result in emission currents that vary during the electron energy scans. Therefore, the emission current must be chosen carefully. In order to determine the maximum possible emission current, we recorded the QMS signal for $O^+$ ions as a function of emission current for different electron energies over the range of 15.7–18.7 eV, as shown in Fig. 4. In Fig. 4, the dotted line connects the points on the constant electron energy curves corresponding to the maximum emission current for which the QMS signal increases linearly with increasing emission

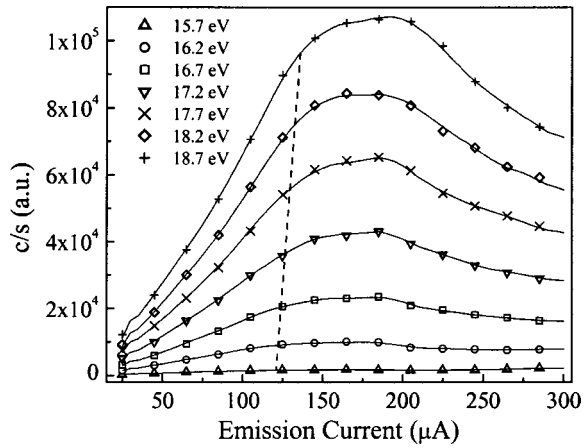


FIG. 4. QMS signal for $Ar^+$ ($m/e=40$) as a function of the electron emission current for different electron energies. The feed–gas composition was 50% $O_2$ and 50% Ar with a pressure of 25 mTorr in the plasma chamber. The dashed line connects points on the constant electron-energy curves corresponding to the maximum emission current for which the QMS signal is linear with respect to the emission current. The nonlinear behavior in each curve, to the right of the dashed line, indicates the onset of space charge in the ionizer of the QMS.

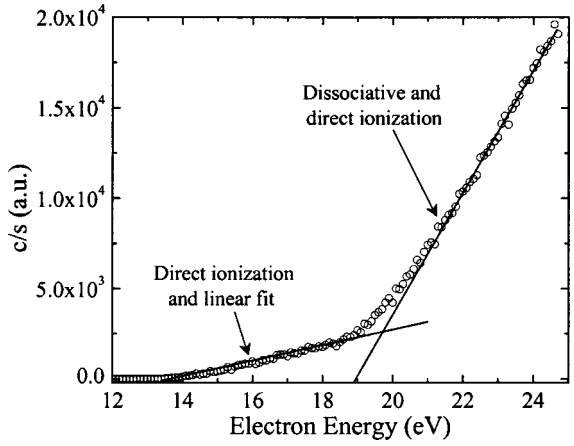


FIG. 5. QMS signal for $O^+$ ($m/e=16$) as a function of electron energy showing the signal from direct and dissociative ionization of O and $O_2$, respectively, and the linear fit for the direct ionization signal. The feed–gas composition was 90% $O_2$ and 10% Ar and the plasma was maintained at a pressure of 100 mTorr.

current. The x intercept of the dotted line in Fig. 4 indicates the maximum allowable emission current in the ionizer to ensure that the ionizer is not operated in the space-charge regime.[12,13] In our experiments, we used an emission current of 120 $\mu$A as determined from the data in Fig. 4.

### C. Calibration of the QMS signal and data collection procedure

In this study, we have used a calibration procedure similar to the one recommended by Singh, Coburn, and Graves[8,9] with further correction to account for the neutral–neutral collisions in the beam during its extraction from the plasma chamber. We shall show later in this article (Sec. IV A) that this correction becomes significant for pressures greater than 75 mTorr in the plasma chamber, where the mean free path, $\lambda_{mf}$, becomes shorter than the orifice diameter (1 mm).

Briefly, the signal, $S$, in counts/s, recorded by the QMS can be written as

$$S=\alpha\cdot I_e\cdot\sigma(E)\cdot n_{\text{ionizer}}, \tag{3}$$

where $I_e$ is the emission current in the ionizer, $\sigma(E)$ is the electron energy dependent cross section of the relevant ionization process, $n_{\text{ionizer}}$ is the number density of the neutral species of interest in the ionizer, and $\alpha$ is a product of the extraction efficiency of the ions from the ionizer, $\beta$, the species mass-to-charge ratio dependent transmission efficiency of the quadrupole mass filter, $T(m/e)$, the species mass-to-charge ratio dependent sensitivity of the SEM, $\theta(m/e)$, and the length of the ionizer cage, $l_{\text{cage}}$ ($\alpha=\beta\cdot T\cdot\theta\cdot l_{\text{cage}}$). Thus, the signal, $S$, for $O^+$ ions, can be expressed as

$$S^{O\rightarrow O^+}(E) = \beta^{O\rightarrow O^+}\cdot T(m_{O^+})\cdot\theta(m_{O^+})\cdot l_{\text{cage}}\cdot I_e\cdot\sigma^{O\rightarrow O^+}\cdot n_O^{\text{on}}. \tag{4}$$

Here, the instrument dependent factors $\beta$, $T(m/e)$, and $\theta(m/e)$ are unknown.

The absolute density of the O radicals in the ionizer, $n_O^{\text{on}}$, can be determined from the QMS signal, $S^{O\rightarrow O^+}$, by using a reference gas and the following calibration procedure. In this study, as the reference signal, we have used the signal from direct ionization of $CH_4$ at a known pressure under plasma-off condition, since $CH_4$ has the same mass as O radicals; the factors $\beta$, $T(m/e)$, and $\theta(m/e)$ are expected to be identical for both $CH_4$ and O. An expression similar to Eq. (4) can be written for the signal from $CH_4^+$ ions

$$S^{CH_4\rightarrow CH_4^+}(E)=\beta^{CH_4\rightarrow CH_4^+}\cdot T(m_{CH_4^+})\cdot\theta(m_{CH_4^+})\cdot l_{\text{cage}}\cdot I_e \cdot\sigma^{CH_4\rightarrow CH_4^+}\cdot n_{CH_4}^{\text{off}}. \tag{5}$$

Dividing Eq. (3) by Eq. (4) and rearranging we get

$$\frac{n_O^{\text{on}}}{n_{CH_4}^{\text{off}}}=\left(\frac{S^{O\rightarrow O^+}}{S^{CH_4\rightarrow CH_4^+}}\right)\cdot\left(\frac{\sigma^{CH_4\rightarrow CH_4^+}}{\sigma^{O\rightarrow O^+}}\right). \tag{6}$$

In Eq. (6), $n_{CH_4}^{\text{off}}$ is proportional to the $CH_4$ pressure in the plasma chamber and can be calculated from the ideal gas law. The relevant cross sections, $\sigma^{CH_4\rightarrow CH_4^+}$ and $\sigma^{O\rightarrow O^+}$, are available from the literature and, thus, the O radical density, $n_O^{\text{on}}$, can be calculated using Eq. (6). Since the cross sections for electron impact ionization processes are linear up to several electron volts above the threshold energy,[28,29] the slope of a linear fit to the QMS signal as a function of electron energy is proportional to the radical density. Figure 5 shows a linear fit for $O^+$ ions for the beam component of the direct ionization signal. Using the linear fit, we have calculated the QMS signal at an energy of 15.7 eV for both $O^+$ ions and $CH_4^+$ ions. The cross sections for direct ionization of atomic O (Ref. 30) and $CH_4$ (Ref. 31), used in our calculations are $7.5\times10^{-18}$ and $1.4\times10^{-17}$ $cm^{-2}$, respectively. We have used the QMS signal at 15.7 eV calculated from the linear fit

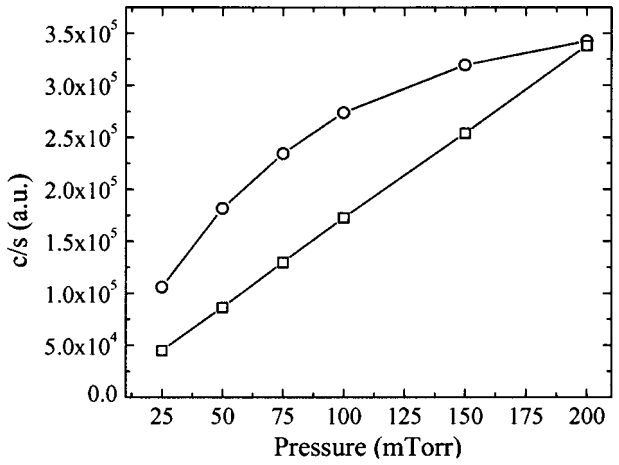


FIG. 6. Beam (○) and background (□) components of the QMS signal for $CH_4^+$ as a function of $CH_4$ pressure in the plasma chamber. During these measurements the plasma was kept off and the QMS electron-energy was 15.8 V.

instead of the actual value at this energy in order to average over more points and to reduce the noise level in the data.

Figure 6 shows the beam and the background components for the QMS signal for the calibration gas, $CH_4$, as a function of pressure in the plasma chamber when the plasma was kept off. Ideally, the beam signal should increase linearly with increasing pressure if there are no neutral–neutral collisions in the beam after it is extracted from the orifice on the substrate stage. Over the pressure range explored in this study (25–200 mTorr), the mean free path will become small enough above some pressure that there are neutral–neutral collisions that result in the scattering of neutrals in the beam before it reaches the QMS ionizer. This scattering results in the attenuation of the beam signal with increasing pressure. Indeed, Fig. 6 shows that the beam component of the QMS signal increases sublinearly with pressure, whereas a linear increase is expected for a perfect collisionless beam. The same effect was observed for both $O_2$ and Ar for nearly identical pressures in the plasma chamber. Figure 6 also shows that the background component increases linearly as a function of pressure in the plasma chamber; this observation confirms that the sublinear increase in the beam signal with increasing pressure is due to a collisional beam and not due to changes in the QMS detection. Furthermore, we confirmed that the attenuation of the beam signal with increasing pressure in the plasma chamber is not due to the saturation of the SEM, since an identical trend was obtained for a higher bias voltage on the SEM detector.

The beam attenuation due to collisions is already taken into account in the calibration procedure to obtain absolute O radical densities since the reference signal, $S^{CH_4 \rightarrow CH_4^+}$, used in Eq. (6) was recorded at each pressure. A separate correction is not required. The reference signal should be recorded immediately after the data for O radical measurements to eliminate the effect of any drift in the sensitivity of the SEM. In our experiments, the $CH_4$ calibration data were recorded on the same day as the O radical measurements. For our QMS, we observed a drift in sensitivity of ~10% over a period of a few weeks.

### D. Calibration of parent-species density and calculation of neutral-gas translational temperature

In a discharge where a radical is generated from the dissociation of the parent molecule, the density of the parent species in the plasma chamber changes when the discharge is turned on. This is true even for low degrees of dissociation because gas heating also affects the neutral densities. In fact, determination of the parent molecule density in addition to the radical density allows calculation of the neutral-gas temperature using the ideal gas law. In order to calculate Ar and $O_2$ densities, we have determined the Ar and $O_2$ beam signals under plasma-on and plasma-off conditions with 35 eV electrons. An example of these data is shown in Figs. 7(a) and 7(b), for $O_2$ and Ar, respectively. Dividing the beam component of the signal for the plasma-on ($S_{i^+}^{\text{on}}$) and plasma-off ($S_{i^+}^{\text{off}}$) conditions gives the fraction of the species ($i = O_2$ or Ar) left in the plasma chamber after the discharge is turned on. Thus,

$$\frac{n_i^{\text{on}}}{n_i^{\text{off}}} = \left.\frac{S_{i^+}^{\text{on}}}{S_{i^+}^{\text{off}}}\right|_{35\ \text{eV}} \quad (i = O_2 \ \text{ or } \ \text{Ar}). \tag{7}$$

The product of this fraction with the density of the species in the plasma-off condition gives the density of Ar and $O_2$ in the plasma when the discharge is turned on. In this calculation, the mole fractions of $O_2$ and Ar in the chamber under the plasma-off condition are assumed to be in the same ratio as in the feed–gas mixture and the Ar and $O_2$ densities are computed using the ideal gas law; the actual ratio in the plasma chamber could be slightly different because of the different pumping speeds for $O_2$ and Ar. The temperature of the gas in the vicinity of the sampling aperture, $T_g$, can then be calculated by using the total neutral density and the measured pressure in the ideal gas law. We have assumed that the pressure at the sampling aperture is the same as the pressure measured at the wall of the plasma chamber. This assumption is very accurate for our chamber geometry over the pressure range used in this study.

## IV. RESULTS AND DISCUSSION

### A. O density

Figure 8 shows a plot of the slopes for the linear fit to the QMS signal in the direct ionization region (see Fig. 5) as a function of pressure for two different $O_2$-to-Ar feed–gas ratios (30% $O_2$ and 100% $O_2$ in feed gas). The slope in the direct ionization region is proportional to the radical density in the plasma. For both $O_2$-to-Ar feed–gas ratios shown in Fig. 8, the O radical signal (slope of the $O^+$ signal obtained through the linear fits in the direct ionization region) increases as a function of pressure up to 100 mTorr, appears to peak at 100 mTorr and either decreases as in the case of 100% $O_2$ or remains constant as in the case of 30% $O_2$ in Ar. However, these trends in radical densities, obtained solely on

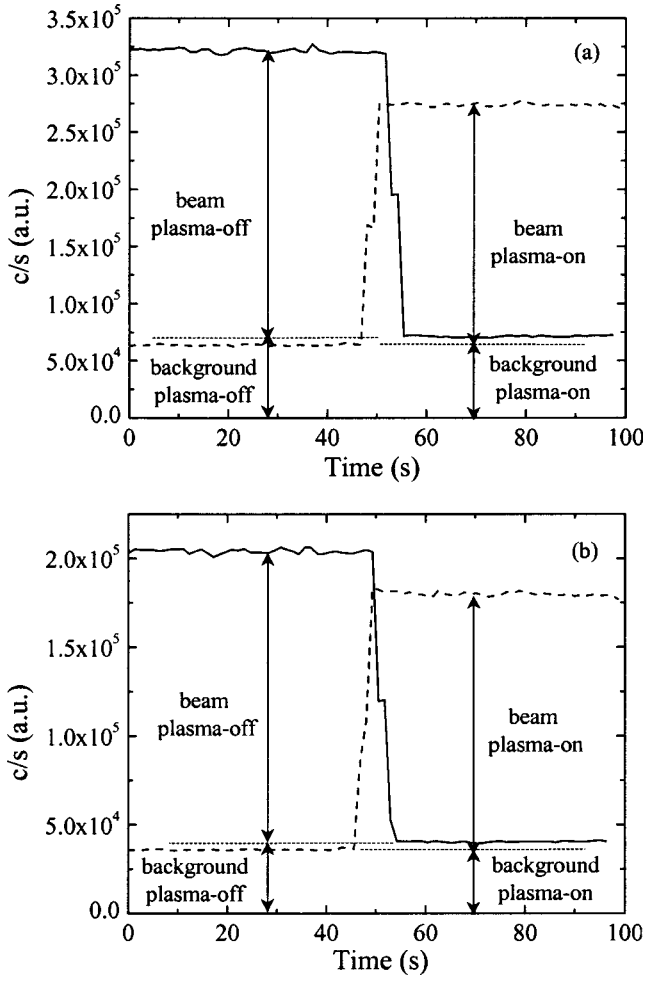


FIG. 7. QMS signal for chopper-open and chopper-closed positions under plasma-on (- - -) and plasma-off conditions (—) for (a) $O_2$ and (b) Ar. The signals for the plasma-on and plasma-off conditions were not collected simultaneously, but have been superimposed on the same plots for comparison. At ~50 s, the chopper position was changed from "closed" to "open" for collecting the QMS signal for the plasma-on condition while the chopper position was changed from "open" to "closed" for collecting the QMS signal for the plasma-off condition. The dotted lines (· · · ·) to the left and right indicate the background levels under the plasma-off condition and plasma-on conditions, respectively. The feed–gas composition was 50% $O_2$ and 50% Ar with 25 mTorr pressure in the plasma chamber.

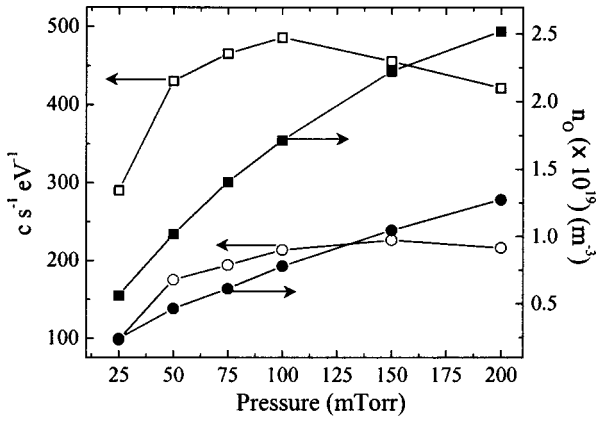


FIG. 8. Slopes of the linear fits (e.g., as in Fig. 5) for the electron energy scans for O as a function of pressure in the plasma chamber for two different feed–gas compositions (left ordinate): 30% $O_2$, 70% Ar (●), and 100% $O_2$ (■). The corresponding absolute O radical density is plotted (right ordinate) as a function of pressure for the same two feed–gas compositions: 30% $O_2$, 70% Ar (○), and 100% $O_2$ (□).

the basis of the raw QMS signal, are misleading since this signal should also be corrected for the increasing number of collisions in the beam at higher pressures in the plasma chamber. The absolute O radical densities, after calibration for this effect as described in Sec. III C, are also shown in Fig. 8 with the O density plotted on the right ordinate. The calibration procedure corrects for signal attenuation due to the radical scattering through collisions. The corrected data show that, unlike the raw data, the O radical signal continues to increase monotonically with increasing pressure. It is clear from the comparisons in Fig. 8 that misleading trends in the radical densities will be obtained if corrections are not made to account for collisions in the beam.

Figure 9 shows the absolute O radical densities as a function of $O_2$-to-Ar feed–gas ratio for different pressures in the plasma chamber. The O radical density varies from 2.1 $\times 10^{18}$ to $2.6 \times 10^{19}$ $m^{-3}$ over the range of the parameters studied. In general, O density was higher for higher pressures and increased with increasing $O_2$-to-Ar ratio in the feed gas. Interestingly, Ar dilution of $O_2$ results in a higher degree of $O_2$ dissociation and the reduction in O density upon Ar dilution is not as much as that would be expected from simple dilution. It is possible to control the O density over an order of magnitude by varying the process conditions such as the pressure and feed–gas composition. Measurements such as these are necessary to maximize the flux of O radicals in various processes in the microelectronics industry, such as deposition of metal oxides through plasma-assisted chemical vapor deposition, photoresist etching, and surface cleaning.

Argon dilution of $O_2$ can affect $O_2$ dissociation through either an increased electron density in the plasma or by dissociation of $O_2$ molecules due to collisions with metastable Ar atoms (Ar*) that carry ~11.6 eV of energy above the ground state. Our results for O radical measurements as a function of Ar dilution are consistent with previous studies in

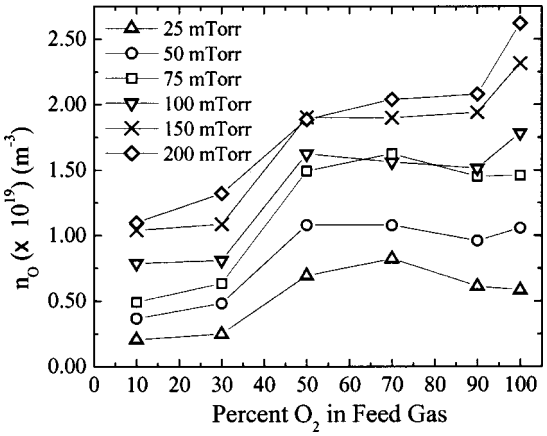


FIG. 9. Absolute density of O radicals as a function of $O_2$ mole percentage in the feed gas for different pressures.

TABLE I. Ratios of $O_2$ and Ar densities under the plasma-on condition to the $O_2$ and Ar densities under the plasma-off condition ($r = S_i^{on}/S_i^{off}$; $i = O_2, Ar$) as a function of the feed–gas composition and chamber pressure.

| Percent $O_2$ in feed gas | Pressure (mTorr) | | | | | | | | | | | |
|---|---|---|---|---|---|---|---|---|---|---|---|---|
| | 25 | | 50 | | 75 | | 100 | | 150 | | 200 | |
| | $O_2$ | Ar | $O_2$ | Ar | $O_2$ | Ar | $O_2$ | Ar | $O_2$ | Ar | $O_2$ | Ar |
| 10 | 0.78 | 0.93 | 0.83 | 0.98 | 0.87 | 0.99 | 0.88 | 0.99 | 0.91 | 0.98 | 0.94 | 1.00 |
| 30 | 0.83 | 0.89 | 0.88 | 0.95 | 0.94 | 0.99 | 0.96 | 1.00 | 0.98 | 1.01 | 1.00 | 1.02 |
| 50 | 0.82 | 0.89 | 0.91 | 0.96 | 0.89 | 0.98 | 0.96 | 0.99 | 0.97 | 0.99 | 1.02 | 1.04 |
| 70 | 0.82 | 0.88 | 0.93 | 0.96 | 0.97 | 0.99 | 0.98 | 1.00 | 1.00 | 1.02 | 0.99 | 1.00 |
| 90 | 0.82 | 0.85 | 0.94 | 0.96 | 0.96 | 0.98 | 0.95 | 0.96 | 0.96 | 0.98 | 1.01 | 1.01 |
| 100 | 0.84 | | 0.95 | | 0.95 | | 0.97 | | 0.97 | | 0.98 | |

the literature, where O radical density in an $O_2$ plasma was studied as a function of inert gas dilution. Booth *et al.* used optical emission actinometry to measure O radical density in an $O_2$/Kr plasma and reported a 100% increase in O radical density for 20% Kr in the feed gas.[32] Furthermore, their measurements showed that there was no change in the electron energy distribution function due to Kr dilution. These authors, therefore, suggested that the increased dissociation of $O_2$ due to Kr dilution was a result of reaction of $O_2$ molecules with Kr metastables that have an energy of $\sim 10$ eV above the ground state. Takechi *et al.* modeled an Ar/$O_2$ plasma with a two-dimensional geometry to account for the effect of Ar dilution of $O_2$ in photoresist etching studies.[33] The simulations of these authors showed that 50% addition of Ar to $O_2$ increases the electron density in the plasma by a factor of 2 compared to a pure $O_2$ plasma. Upon Ar dilution, an increase in etch rate of the photoresist was also observed in the experiments conducted by Takechi *et al.* The increased etch rate was attributed to an increase in the electron density in the plasma and enhancement of O-atom density by dissociation of $O_2$ by Ar*.

For all the data presented in this section, three measurements were made. The first measurement was made immediately after the plasma was turned on and then after 30 and 60 min, respectively, of plasma-on time. We found that the O radical signal changes slowly during the first 30 min and then stabilizes. The data obtained after 30 and 60 min of plasma-on time were within 15% of each other. The values used in our calculations are an average of the data recorded after the plasma has remained on for 30 and 60 min. The most likely reason for the change in the O-radical signal was a drift in the chamber wall temperature after the discharge was turned on, particularly of the quartz window through which rf power was coupled to the discharge. Over the plasma chamber pressure range investigated in this study, radical recombination occurs primarily on the surfaces. Chamber wall temperature affects the recombination coefficient of the radicals and, thus, the radical density in the plasma volume until the wall temperature is stabilized. The maximum error in the O-radical density measurements was $\pm 16\%$. This does not include the systematic errors in the electron-impact ionization cross sections in the literature.

### B. $O_2$ and Ar density and neutral gas temperature

The ratio, $r$, of $O_2$ and Ar densities in the plasma chamber under the plasma-on condition to the $O_2$ and Ar densities under the plasma-off condition, i.e., $S_i^{on}/S_i^{off}(i = O_2, Ar)$, are summarized in Table I, for the different pressures and $O_2$-to-Ar feed–gas ratios investigated in this study. Both $O_2$ and Ar densities are expected to decrease when the plasma is turned on due to the dissociation of $O_2$ molecules and due to the expected increase in the neutral-gas temperature, $T_g$. If the pressure in the chamber remains uniform and equal to the measured pressure after the discharge is turned on, an increase in $T_g$ will lower the number density of the gas molecules in the chamber according to the ideal gas law. In the data shown in Table I, at 150 and 200 mTorr, for all $O_2$-to-Ar feed–gas ratios, there is no significant change in the Ar density: the values for $r$ range from 0.98 to 1.04. A value higher than unity is not expected because neutral gas heating should reduce the mole fraction of the gas when the discharge is turned on. Therefore, based on this argument, we estimate a maximum error of $\pm 4\%$ for the data in Table I.

At pressures less than 150 mTorr and low $O_2$-to-Ar feed–gas ratios, there is a significant decrease (up to 22%) in the density of $O_2$ when the discharge is turned on. In addition, this decrease in the $O_2$ density is much greater than that for Ar. The greater reduction in the density of $O_2$ compared to that for Ar cannot be attributed to $O_2$ dissociation to form O atoms. The mole fraction of $O_2$ dissociated in the plasma calculated using $0.5 \times n_O^{on}/(n_{O_2}^{on} + 0.5 \times n_O^{on})$, never exceeded 1.5%. Thus, the larger decrease in the $O_2$ density has to be attributed to a higher translational temperature of $O_2$ molecules compared to that for Ar atoms. Since the $O_2$ translational temperature is higher than that for Ar, there must be preferential heating mechanisms for $O_2$ molecules, in conjunction with an insufficient number of collisions between these ''hot'' $O_2$ molecules and Ar atoms for the two species to reach complete thermal equilibrium. Thus, from the data shown in Table I, it is apparent that it would be incorrect to simply use the change in parent-molecule mole fraction to calculate the density of the corresponding atomic species in the plasma since there can be substantial reduction in the density of the parent species due to a rise in $T_g$. Further-

more, our data also show that it would be incorrect to use the change in the density of a monoatomic specie like Ar for calibrating the neutral-gas temperature, since the translational temperatures of Ar and $O_2$ may not be in equilibrium with each other, as is the case in our measurements.

The primary heating mechanisms for $O_2$ and Ar in the plasma are (a) elastic and charge–exchange ion–neutral collisions in the presheath; (b) vibrational and rotational excitation of molecular species by electron-impact and subsequent vibrational–translational (V–T) and rotational-translational (R–T) relaxation through gas–phase collisions with ground-state neutrals; (c) formation of excited molecules due to exothermic radical–radical recombination reactions on the chamber walls; and (d) Franck–Condon heating of the neutral fragments generated by electron impact dissociation of molecules and subsequent exchange of their excess energy with $O_2$ and Ar in the plasma through gas-phase collisions. The excited molecules formed by process "c" can have several electron volts of translational and internal (vibrational, rotational, and electronic) energy. However, most of this excess energy is expected to be in the vibrational levels.[34] The V–T relaxation for highly vibrationally excited states of $O_2$ which may be formed in process "c" is efficient because these states are anharmonic and, therefore, during collisions with ground-state $O_2$ molecules, the vibrational–vibrational (V–V) relaxation process is nonresonant. For example, the V–V relaxation reaction between two vibrationally excited $O_2$ molecules:

$$O_2^v + O_2^j \rightarrow O_2^{v-1} + O_2^{j+1}, \tag{8}$$

where both $v$ and $j$ are vibrational quantum numbers, will be nonresonant if $v$ and $j$ are not approximately equal. This will be the case for collisions in low-temperature plasmas, where most collisions of a vibrationally excited $O_2$ molecule will be with ground-state $O_2$ molecules. Thus, for anharmonic oscillators, an amount of energy, $\Delta E = E_{v,v-1} - E_{j+1,j}$ is removed from vibration to translation according to the reaction

$$O_2^v + M \rightarrow O_2^{v-1} + M, \tag{9}$$

where species M could be ground-state $O_2$ or Ar, leading to neutral gas heating. Due to the complexity of the different heating mechanisms and the lack of reliable rate coefficients for the different gas phase and surface processes, it is not possible to quantify the contribution of each mechanism mentioned above for the heating of different species in even the simplest of plasma gases. Therefore, we will only qualitatively discuss the most likely mechanism for the higher translational temperature of $O_2$ compared to that for Ar.

In an $O_2$ plasma, heating due to excitation of vibrational levels of $O_2$ by electron impact and subsequent V–T relaxation (process "b") is not an important source of heating due to the small electron-impact vibrational cross section of $O_2$.[34] According to the model developed by Pinheiro *et al.*,[34] the primary causes for gas heating in an $O_2$ discharge are vibrationally excited species created by atomic recombination on the chamber walls (process "c") and Franck–Condon heating (process "d"). The excess internal energy or

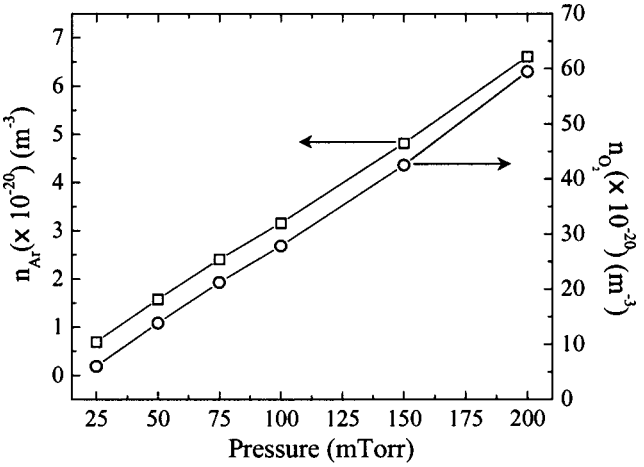


FIG. 10. Density of $O_2$ (○) and Ar (□) as a function of pressure in the plasma chamber for an $O_2$-to-Ar feed–gas ratio of 9:1. The plasma power was maintained at 500 W.

kinetic energy from the above processes is then released to other ground-state atomic and molecular species via collisions. During relaxation by collisions, the vibrational energy released into the translational energy is shared by both colliding species and each one receives a fraction of this energy depending on its atomic mass. For example, during a collision of a vibrationally excited species A, of mass $m_A$, with a ground-state species B, of mass $m_B$, the vibrational or rotational energy released into kinetic energy, $\Delta E$, will be shared by species A and B as, $\Delta E \times m_B/(m_A+m_B)$ and $\Delta E \times m_A/(m_A+m_B)$, respectively.[35] Thus, during relaxation of vibrationally excited $O_2$ through collisions with ground-state Ar, $O_2$ will receive ~12% more translational velocity. For the case of $O_2$ and Ar heating through collisions of excited O atoms formed by Franck–Condon heating, again, $O_2$ will get more translational velocity than Ar, thus resulting in preferential heating of $O_2$ molecules. However, the number of gas–phase collisions has to be insufficient for complete translational relaxation of $O_2$ and Ar, which is the case at pressures below 150 mTorr in our experiments. The translational temperatures of $O_2$ and Ar are well equilibrated above this pressure.

To estimate the *average* neutral-gas temperature, the absolute number densities of $O_2$ and Ar have to be determined. Figure 10 shows the absolute densities of $O_2$ and Ar as a function of pressure in the plasma chamber for an $O_2$-to-Ar feed-gas ratio of 9:1 with the discharge turned on. The densities shown in Fig. 10 were simply obtained from the product of the ratio, $r$, in Table I and the number density of $O_2$ and Ar with the discharge turned off, at the relevant pressure and feed–gas ratio. In calculating the number densities of $O_2$ and Ar with the discharge turned off, we have assumed that the ratio of partial pressures of $O_2$ to Ar is the same as their ratio in the feed gas. Since the pumping speeds of $O_2$ and Ar are different, this introduces a maximum error of 12% in the determination of their absolute densities with the discharge turned off. It should be noted that the data in Table I do not contain any error due to the difference in pumping speeds on

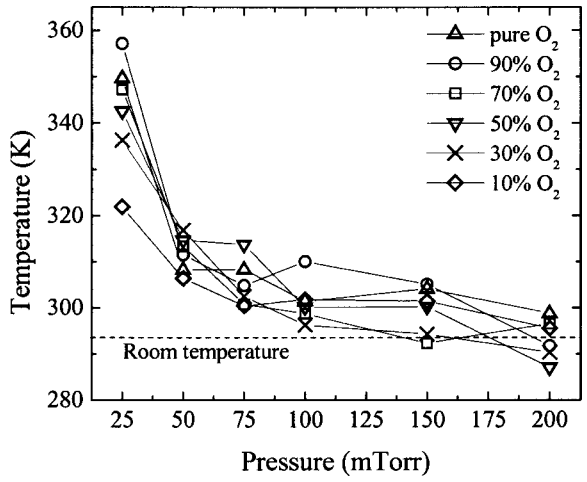


FIG. 11. Average neutral-gas temperature, $T_g$, as a function of pressure for different $O_2$-to-Ar feed-gas ratios.

$O_2$ and Ar; this is because these are simply the ratios of the density of $O_2$ and Ar after the discharge is turned on to their density with the discharge turned off.

The *average* neutral-gas temperature, $T_g$, calculated using the measured pressure and the total number density of neutrals ($n_{\text{total}}=n_O+n_{O_2}+n_{Ar}$) is plotted in Fig. 11 as a function of pressure for all of the $O_2$-to-Ar feed–gas ratios examined. The maximum error in the calculation of $T_g$ was estimated to be $\pm 13\%$. The highest gas temperatures (320–360 K) were recorded at low pressures and low $O_2$-to-Ar feed–gas ratios. This is consistent with the gas heating mechanism ''c'' discussed above. At low pressures, the diffusion loss of O radicals to the chamber walls is greater resulting in a higher O–O wall-recombination rate and, thus, a higher generation rate for vibrationally excited $O_2$ molecules that cause gas heating. The heating of the neutral gas is the least at the lowest $O_2$-to-Ar feed-gas ratio for a pressure of 25 mTorr. This also corresponds to the lowest steady-state O radical density at this pressure, which implies a lower wall-recombination rate for O radicals.

## V. CONCLUSIONS

We have designed, developed, and demonstrated an experimental apparatus for measuring the density of radicals and parent species as well as the neutral-gas temperature in a plasma using modulated beam LOS-TIMS. The QMS was placed in a three-stage differentially pumped vacuum chamber and the extracted molecular beam was modulated with a chopper placed in between the sampling aperture and the QMS in the second stage of differential pumping in order to separate the beam and background components of the ion signal. In our design and calibration we have accounted for various sources of error such as, the contribution to the QMS signal from the background gases, the ion mass-to-charge ratio dependent sensitivity of the various components of the QMS, space-charge limitations in the QMS ionizer, and collisions within the molecular beam extracted from the discharge particularly at higher pressures ($>75$ mTorr). Absolute O, $O_2$, and Ar densities and the *average* neutral-gas temperature were determined near the substrate plane as a function of pressure in the plasma chamber (25–200 mTorr) and the mole percent of Ar in $O_2$ (0%–90%). We have found that the O atom density increases with pressure and $O_2$ mole fraction in the feed gas and is over the range of $2.1\times10^{18}-2.6\times10^{19}$ m$^{-3}$. At low pressures, our measurements showed that the $O_2$ translational temperature is higher than that for Ar.

## ACKNOWLEDGMENTS

This work has been supported by the NSF/DOE Partnership for Basic Plasma Science and Engineering (Award No. ECS-0078711). Several insightful discussions with Dr. W. M. M. Kessels, the technical assistance of Andy Segale and Rudy Stöber at UCSB for the QMS housing fabrication, as well as useful discussions regarding the QMS operation and maintenance with Dr. Claire Greenwood at Hiden Analytical Ltd. are gratefully acknowledged. G.W.W.Q. acknowledges financial support from the Eindhoven University of Technology.

[1]O. Auciello and D. L. Flamm, *Plasma Diagnostics* (Academic, New York, 1989).
[2]P. Kae-Nune, J. Perrin, J. Guillon, and J. Jolly, Plasma Sources Sci. Technol. **4**, 250 (1995).
[3]R. Robertson, D. Hils, H. Chatham, and A. Gallagher, Appl. Phys. Lett. **43**, 544 (1983).
[4]R. Robertson and A. Gallagher, J. Appl. Phys. **59**, 3402 (1986).
[5]P. Kae-Nune, J. Perrin, J. Guillon, and J. Jolly, Jpn. J. Appl. Phys., Part 1 **33**, 4303 (1994).
[6]P. Kae-Nune, J. Perrin, J. Jolly, and J. Guillon, Surf. Sci. **360**, L495 (1996).
[7]J. Perrin, M. Shiratani, P. Kae-Nune, H. Videlot, J. Jolly, and J. Guillon, J. Vac. Sci. Technol. A **16**, 278 (1998).
[8]H. Singh, J. W. Coburn, and D. B. Graves, J. Vac. Sci. Technol. A **17**, 2447 (1999).
[9]H. Singh, J. W. Coburn, and D. B. Graves, J. Vac. Sci. Technol. A **18**, 299 (2000).
[10]H. Sugai and H. Toyoda, J. Vac. Sci. Technol. A **10**, 1193 (1992).
[11]V. M. Donnelly, J. Appl. Phys. **79**, 9353 (1996).
[12]C. M. Leewis, M. S. thesis, Eindhoven University of Technology, 1999.
[13]W. M. M. Kessels (private communication).
[14]M. F. Harrison, Br. J. Appl. Phys. **17**, 371 (1966).
[15]A. P. Wynter and J. B. Hasted, J. Phys. E **7**, 627 (1974).
[16]H. Singh, J. W. Coburn, and D. B. Graves, J. Vac. Sci. Technol. A **19**, 718 (2001).
[17]S. Agarwal, A. Takano, M. C. M. van de Sanden, D. Maroudas, and E. S. Aydil, J. Chem. Phys. **117**, 10805 (2002).
[18]J. D. Allen, Jr., J. P. Wolfe, and G. K. Schweitzer, Int. J. Mass Spectrom. Ion Phys. **8**, 81 (1972).
[19]J. D. Allen, Jr., J. D. Durham, G. K. Schweitzer, and W. E. Deeds, J. Electron Spectrosc. Relat. Phenom. **8**, 395 (1976).
[20]P. Clausing, Z. Phys. **66**, 471 (1930).
[21]J. H. Craig and J. L. Hock, J. Vac. Sci. Technol. **17**, 1360 (1980).
[22]J. H. Craig and W. G. Durrer, J. Vac. Sci. Technol. A **7**, 3337 (1989).
[23]H. Yoshikawa and R. Shimizu, Jpn. J. Appl. Phys., Part 1 **29**, 386 (1990).
[24]H. Singh, J. W. Coburn, and D. B. Graves, J. Appl. Phys. **88**, 3748 (2000).
[25]K. L. Bell, H. B. Gilbody, J. G. Hughes, A. E. Kingston, and F. J. Smith, J. Phys. Chem. Ref. Data **12**, 891 (1983).
[26]E. Krishnakumar and S. K. Srivastava, Int. J. Mass Spectrom. Ion Processes **113**, 1 (1992).
[27]I. Langmuir and K. B. Blodgett, Phys. Rev. **22**, 347 (1923).
[28]S. Geltman, Phys. Rev. **102**, 171 (1956).
[29]M. R. H. Rudge and M. J. Seaton, Proc. R. Soc. A **283**, 262 (1965).

[30]W. R. Thompson, M. B. Shah, and H. B. Gilbody, J. Phys. B **28**, 1321 (1995).
[31]O. J. Orient and S. K. Srivastava, J. Phys. B **20**, 3923 (1987).
[32]J. P. Booth, O. Joubert, J. Pelletier, and N. Sadeghi, J. Appl. Phys. **69**, 618 (1991).
[33]K. Takechi and M. A. Lieberman, J. Appl. Phys. **90**, 3205 (2001).
[34]M. J. Pinheiro, B. F. Gordiets, and C. M. Ferreira, Plasma Sources Sci. Technol. **8**, 31 (1999).
[35]J. B. Hasted, *Physics of Atomic Collisions*, 2nd ed. (Butterworths, London, 1972).